Elimination of degeneracy in the γ-unstable Bohr Hamiltonian in the presence of an extended sextic potential

Hassan Hassanabadi and Hadi Sobhani[*]

Faculty of Physics, Shahrood University of Technology, P.O. Box 3619995161-316, Shahrood, Iran

In this paper, the γ-unstable Bohr Hamiltonian is studied in the presence of an extended sextic potential. It is expected that in this situation, we reach some degenerate levels in the energy spectrum, but we are interested in a case in which there is no degeneracy between those levels. This goal can be achieved by including the effects of an interaction made by the Casimir operator of SO(3). When this term is involved in the γ-unstable Bohr Hamiltonian, the degeneracy will be removed. According to the new scheme of energy levels, after the elimination of degeneracy, some low-lying excited levels are introduced. Then we examine the results by reproducing the experimental data of some isotopes for energy levels and $E2$ electromagnetic transitions.

I. INTRODUCTION

Describing the critical point symmetries in atomic nuclides and the shape transition of the interacting Boson model can be investigated by exact or approximate analytical solutions of the equation of the Bohr Hamiltonian with some physical potential models [1–4]. The critical point symmetries have been confirmed experimentally and they include X(5) [5–10] and E(5) [11–15]. The first order phase transition between spherical and prolate deformed nuclei [7] is related to X(5) symmetry, while E(5) symmetry corresponds to the second order phase transition between spherical and γ-unstable nuclei. However, in E(5) symmetry the potential model is totally independent of the collective γ variable, whereas the potential model in X(5) symmetry can be separated into two linearly independent terms, where the γ part is a harmonic oscillator centered around $\gamma = 0$ which corresponds to prolate deformed nuclei and β is the degree of freedom corresponding to the magnitude of the deformation [4,7,16]. However, E(5) symmetry can be viewed as a transition from vibrational U(5) to γ-unstable nuclei O(6) symmetry, while X(5) symmetry corresponds to the transition from the vibrational spherical shape U(5) to the prolate deformed nuclei SU(3) [4,7,16].

In the case of E(5) symmetry, there are some degeneracies between the levels with a specific quantum number (which is called seniority). The degeneracy can be removed if we include the Casimir operator of SO(3) as an interaction. In this paper, we want to consider an extended sextic potential [17] instead of the infinite square well in the Bohr Hamiltonian and we consider the Casimir operator of SO(3) as an interaction as well. According to this goal, we study the analytical solution of the Bohr Hamiltonian and discuss the results. Therefore, we have organized the paper as follows: In Sec. II, we study a generalized form of the γ-unstable form of the Bohr Hamiltonian. Then, the analytical solution for the β part of

the Hamiltonian is derived in detail. Section III includes the numerical results for the considered system, such as the study of the energy scheme, staggering in the γ band, and the $E2$ electromagnetic transition. In the last section of this paper, we collect the conclusions.

II. GENERALIZED γ-UNSTABLE VERSION OF THE BOHR HAMILTONIAN

To describe the structure of even-even nuclei around the critical point of transition between the spherical and deformed γ-soft structure, we can use the Bohr Hamiltonian, which is written in terms of the collective variables as [1,2]

$$
\begin{aligned}
H = -\frac{\hbar^2}{2B} \Bigg[&\frac{1}{\beta^4} \frac{\partial}{\partial\beta} \beta^4 \frac{\partial}{\partial\beta} + \frac{1}{\beta^2 \sin(3\gamma)} \frac{\partial}{\partial\gamma} \sin(3\gamma) \frac{\partial}{\partial\gamma} \\
&- \frac{1}{4\beta^2} \sum_{k=1}^{3} \frac{Q_k^2}{\sin^2\left(\gamma - \frac{2}{3}\pi k\right)} \Bigg] + V(\beta,\gamma),
\end{aligned} \tag{1}
$$

in which the deformation coordinate measuring the departure from the spherical shape is shown by β, γ represents the angle measuring the departure from axial symmetry, $Q_k(k = 1,2,3)$ stands for the operators of the total angular momentum projections in the intrinsic reference, and we have the mass parameter B. In the γ-unstable Bohr Hamiltonian, it is supposed that the potential appearing in the original Bohr Hamiltonian depends only on the variable β. We are interested in considering an extended sextic potential, introduced in Ref. [17]. It can be checked from the previous papers in this literature that, in this case, there are degeneracies between some levels but if we include the Casimir operator of SO(3), $\mathbf{L}.\mathbf{L}$ [18], in the interaction, the degeneracy can be removed. It means that the final form of the potential is

$$
v(\beta,L) = \frac{2B}{\hbar^2} V(\beta,L) = g(\beta)\mathbf{L}.\mathbf{L} + \frac{\kappa^4}{\beta^2} + a\beta^2 + b\beta^4 + c\beta^6, \tag{2}
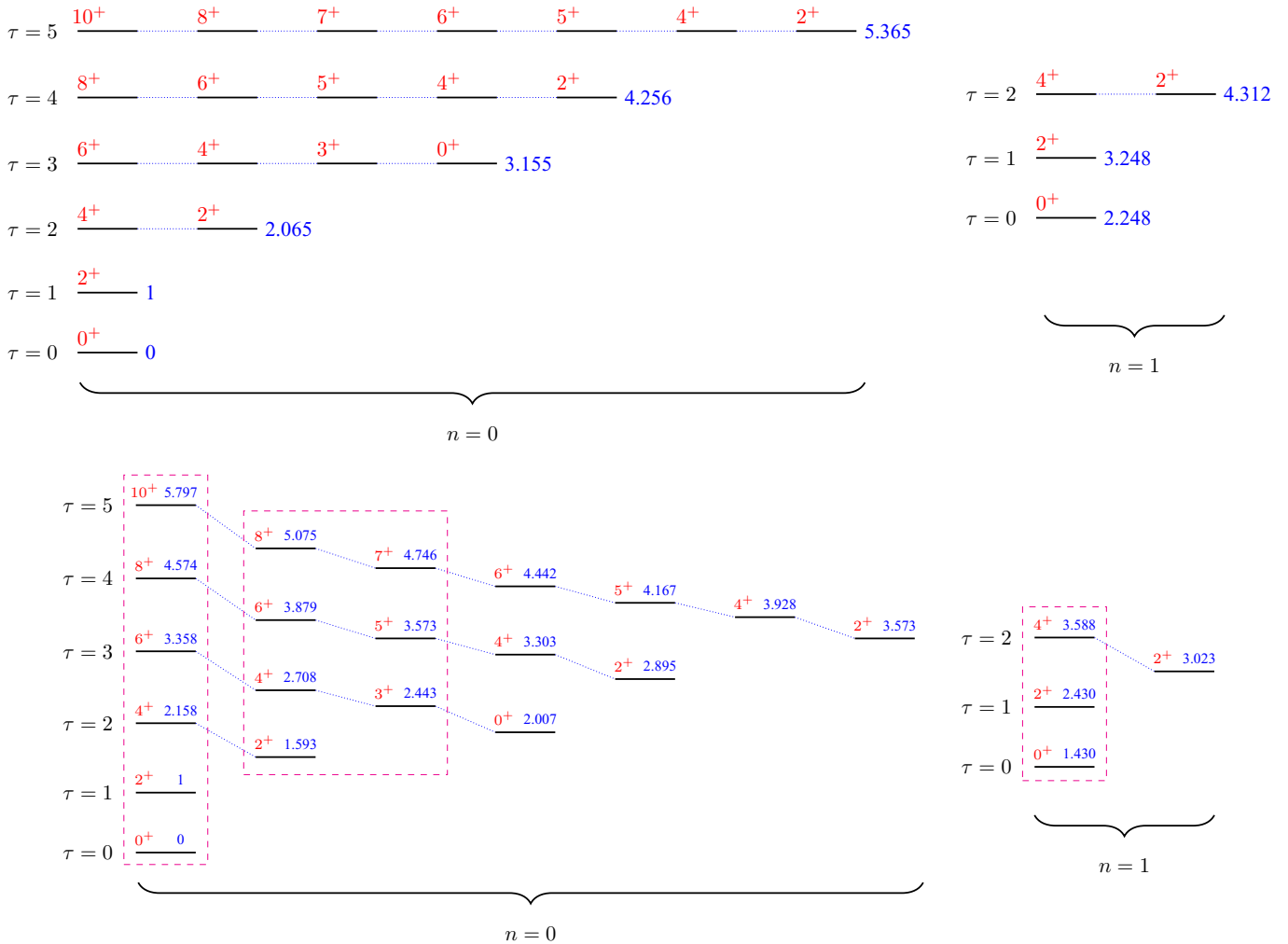$$

* Corresponding author: hadisobhani8637@gmail.com

FIG. 1. The upper plot of this figure shows Eq. (22) when $\kappa = 1$ and $\eta = 0.0$. In this case, there is degeneracy between some levels: those have the same seniority number. The lower plot shows Eq. (22) when $\kappa = 1$ and $\eta = 0.5$. In this case, the degeneracy has been removed. There are three boxes in the lower plot. These boxes show how we should recognize the ground, γ and β bands in the considered model. The values are normalized to the first excited level of the ground band.

where $v(\beta, L)$ is called the reduced potential, and $g(\beta)$ is a general function of β that controls the effects of the Casimir operator of SO(3), which leaves the values of $L(L+1)$ and the free parameters κ, a, b, and c. Considering the wave function in the separable form of $\Phi(\beta, \gamma, \vartheta) = f(\beta)\psi(\gamma, \vartheta)$, where ϑ stands for the Euler angles, we can derive following differential equations [8,9]:

$$\left[-\frac{1}{\sin(3\gamma)} \frac{\partial}{\partial \gamma} \sin(3\gamma) \frac{\partial}{\partial \gamma} + \frac{1}{4} \sum_{k=1}^{3} \frac{Q_k^2}{\sin^2\left(\gamma - \frac{2}{3}\pi k\right)} \right] \psi(\gamma, \vartheta)$$
$$= \Lambda \psi(\gamma, \vartheta), \qquad (3)$$

$$\left[-\frac{1}{\beta^4} \frac{\partial}{\partial \beta} \beta^4 \frac{\partial}{\partial \beta} + \frac{\Lambda}{\beta^2} + v(\beta, L) \right] f(\beta) = \varepsilon f(\beta), \qquad (4)$$

where the reduced energy is $\varepsilon = \frac{2BE}{\hbar^2}$. The solutions of the angular part can be constructed as

$$\psi_{\tau, \tilde{v_\Delta}, L, M_L}(\gamma, \vartheta) = \sum_{\substack{K=0 \\ \text{even}}}^{L} \Gamma_{\tau, \tilde{v_\Delta}, L, K}(\gamma) \phi_{M_L, K}^{L}(\vartheta), \qquad (5)$$

$$\phi_{M_L, K}^{L}(\vartheta) = \sqrt{\frac{2L+1}{16\pi^2(1+\delta_K)}} \left[D_{MK}^{(L)}(\vartheta) + (-)^L D_{M-K}^{(L)}(\vartheta) \right], \qquad (6)$$

where $D(\vartheta)$ is the Wigner function and $\Gamma(\gamma)$ are polynomials containing trigonometric functions of γ. In the equation involving the angles, the eigenvalues of the second order Casimir operator of SO(5) occur, having the form $\Lambda = \tau(\tau + 3)$,

TABLE I. List of quantum numbers for the ground, the first γ, and β bands.

L_{band}	0_g	2_g	4_g	6_g	8_g	10_g	2_γ	3_γ	4_γ	5_γ	6_γ	7_γ	8_γ	0_β	2_β	4_β
n	0	0	0	0	0	0	0	0	0	0	0	0	0	1	1	1
τ	0	1	2	3	4	5	2	3	3	4	4	5	5	0	1	2

where $\tau = 0, 1, \ldots$ is the quantum number characterizing the irreducible representations of SO(5), called the *seniority*.

The radial equation (4) possesses analytic solutions (or dynamical symmetries). For our study, we would like to consider $g(\beta) = \eta/\beta^2$ with a real free parameter η in the potential term. Using an auxiliary function $f(\beta) = u(\beta)/\beta^2$, we have

$$\frac{d^2u(\beta)}{d\beta^2} + \left[\varepsilon - \frac{z(\tau,L)}{\beta^2} - a\beta^2 - b\beta^4 - c\beta^6\right]u(\beta) = 0, \quad (7)$$

$$z(\tau,L) = \tau(\tau + 3) + \eta L(L + 1) + \kappa^4 + 2. \quad (8)$$

Using a new variable $y = \beta^2$, Eq. (7) should be rewritten in order to find its solutions. So we have

$$\frac{d^2u(y)}{dy^2} + \frac{1}{y}\frac{du(y)}{dy} + \left[-\frac{z(\tau,L)}{4y^2} + \frac{\varepsilon}{4y} - \frac{a}{4} - \frac{b}{4}y - \frac{c}{4}y^2\right]u(y) = 0. \quad (9)$$

The next step is using another auxiliary function which can remove the first derivative term in Eq. (9). Introducing $u(y) = \frac{Y(y)}{\sqrt[4]{y}}$, we derive a new differential equation as

$$\frac{d^2Y(y)}{dy^2} + \left[-\frac{z(\tau,L)}{4} - \frac{3}{16}}{y^2} + \frac{\varepsilon}{4y} - \frac{a}{4} - \frac{b}{4}y - \frac{c}{4}y^2\right]Y(y) = 0. \quad (10)$$

We can reach the bi-confluent Heun differential equation using

$$Y(y) = y^A \exp[y(B + Dy)]h(y), \quad (11)$$

$$A = \frac{1}{2} + \frac{1}{2}\sqrt{z(\tau,L) + \frac{1}{4}}, \quad (12)$$

$$B = -\frac{b}{8}, \quad (13)$$

$$D = -\frac{\sqrt{c}}{4}. \quad (14)$$

Substituting Eq. (11) into Eq. (10) and setting $c = 4$, we can derive the bi-confluent Heun differential equation

$$h''(y) + \left(\frac{2A}{y} + 2B - 2y\right)h'(y) + \left(\frac{2AB + \frac{\varepsilon}{4}}{y} + B^2 - \frac{a}{4}\right. $$
$$\left. + 2D(1 + 2A)\right)h(y) = 0, \quad (15)$$

where the prime means derivative with respect to y. The solutions of this differential equation can be written in terms of bi-confluent Heun functions [19], H_b:

$$h(y) = H_b(\alpha', \beta', \gamma', \delta'; y), \quad (16)$$

$$\alpha' = \sqrt{\frac{9}{4} + \tau(\tau + 3) + \eta L(L + 1) + \kappa^4}, \quad (17)$$

$$\beta' = \frac{b}{4}, \quad (18)$$

$$\gamma' = \frac{1}{4}\left(\frac{b^2}{16} - a\right), \quad (19)$$

$$\delta' = \frac{-\varepsilon}{2}. \quad (20)$$

Now, we can write the final form of the β-part wave function in the form of

$$f(\beta) = N_c\beta^{\sqrt{\kappa^4 + \eta L(L+1) + \tau(\tau+3) + \frac{9}{4}} - \frac{3}{2}} \exp\left[-\beta^2\left(\frac{\beta^2}{2} + \frac{b}{8}\right)\right]$$
$$\times H_b(\alpha', \beta', \gamma', \delta'; \beta^2), \quad (21)$$
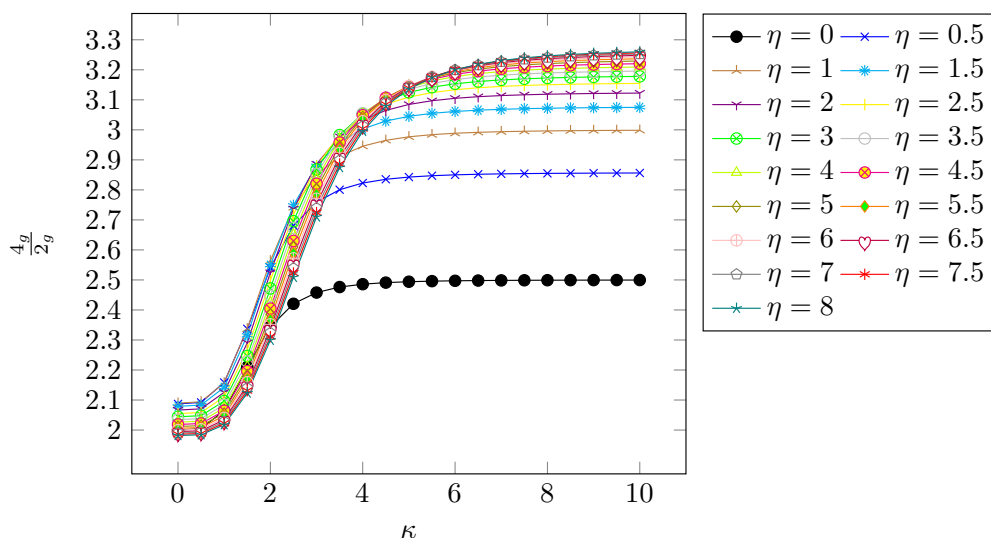

FIG. 2. Behavior of $\frac{4_g}{2_g}$ as a function of the free parameters κ for different values of η.

TABLE II. List of free parameters for each isotope determined in the fitting process. The last column is the deviation of the theoretical prediction determined in the fitting process.

Isotope	κ	η	σ
^{118}Xe	2.01	0.30	0.541
^{120}Xe	2.18	0.38	0.506
^{122}Xe	2.35	0.19	0.251
^{124}Xe	2.19	0.31	0.262
^{126}Xe	2.06	0.32	0.238
^{128}Xe	1.70	0.18	0.138

where the normalization constant is shown by N_c. To derive the energy spectrum of the considered system, we should use the expansion for the differential equation as described in Ref. [20]. We find the energy spectrum along with a constraint as

$$\varepsilon = \frac{b}{2}\left(2n+5+\sqrt{\frac{9}{4}+\tau(\tau+3)+\eta L(L+1)+\kappa^4}\right), \quad (22)$$

$$a = \frac{b^2}{16}-4\left(2n+4+\sqrt{\frac{9}{4}+\tau(\tau+3)+\eta L(L+1)+\kappa^4}\right), \quad (23)$$

where Eq. (23) is needed to determine the wave function through Eq. (19). Having the wave function and energy spectrum, we are in a position to examine the results in the next section.

III. NUMERICAL RESULTS

In this section, special attention will be paid to the energy spectra and $E2$ electromagnetic transition rates of the system discussed in the previous section. As we implied before, including the effects of the Casimir operator of SO(3) in the potential led to an eigenvalue equation in which there was an angular momentum dependent term. Having a term depending on the angular quantum numbers removes the degeneracy in the energy scheme. This point is shown in Fig. 1. In this figure, we compare the results of the two cases of presence and absence of degeneracy in the energy scheme. In the upper plot of Fig. 1, we have used Eq. (22). Actually, the values are normalized to the first excited levels using

$$L_{\text{band}} = \frac{\varepsilon(n,\tau,L)-\varepsilon(0,0,0)}{\varepsilon(0,1,2)-\varepsilon(0,0,0)}. \quad (24)$$

In the upper plot, we set $\kappa = 1$ and $\eta = 0$. This consideration leads to the degenerate case of the γ-unstable Bohr Hamiltonian results. However, in the lower plot of Fig. 1, we set $\kappa = 1$ and $\eta = 0.5$. It is seen that in this case there is no degeneracy like the upper plot. After elimination of degeneracy of the excited levels, we want to classify them into the well-known bands of ground, γ, and β. There are three boxes in the lower plot of Fig. 1. The first box from the left can be considered the ground band. In this band, we have the lowest energy level and its excited levels are constructed by adding two units of angular momentum. The middle box represents the first γ band. In this band, as we know, the angular momentum of each excited level can be constructed by adding one unit of angular momentum. In these bands the quantum number of the β variable, n in
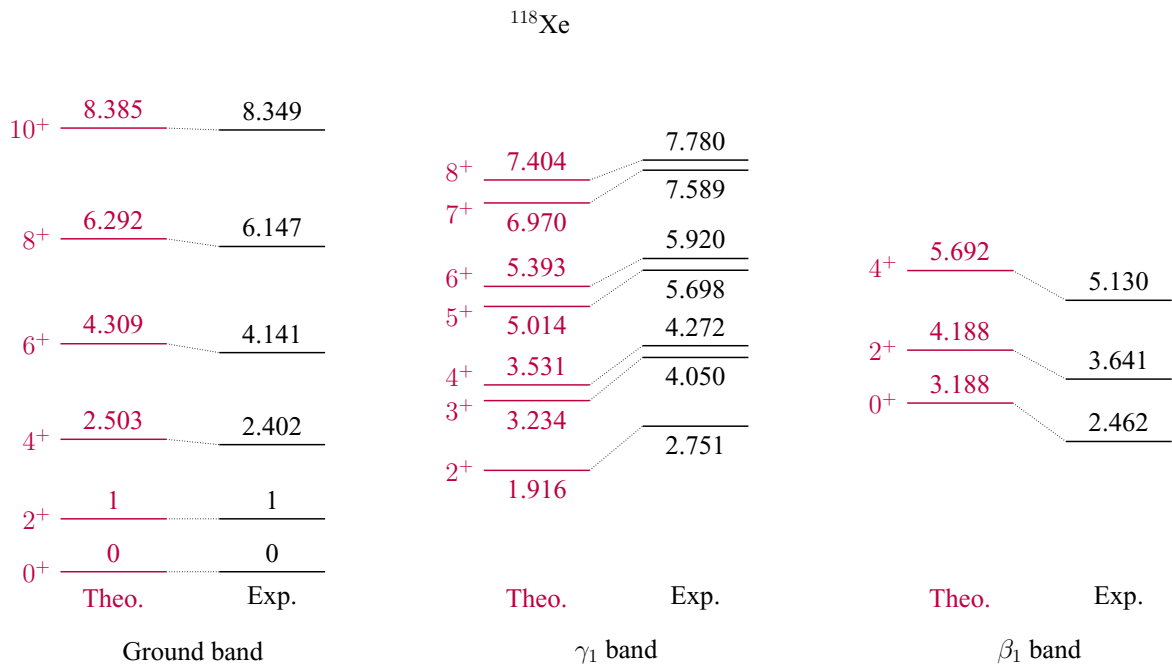
^{118}Xe

FIG. 3. Energy scheme of ^{118}Xe. In the fitting process, we used the levels which are connected to their corresponding experimental values. Experimental data for the energy levels were taken from Ref. [21]. The values have been normalized to the first excited levels of the ground band.
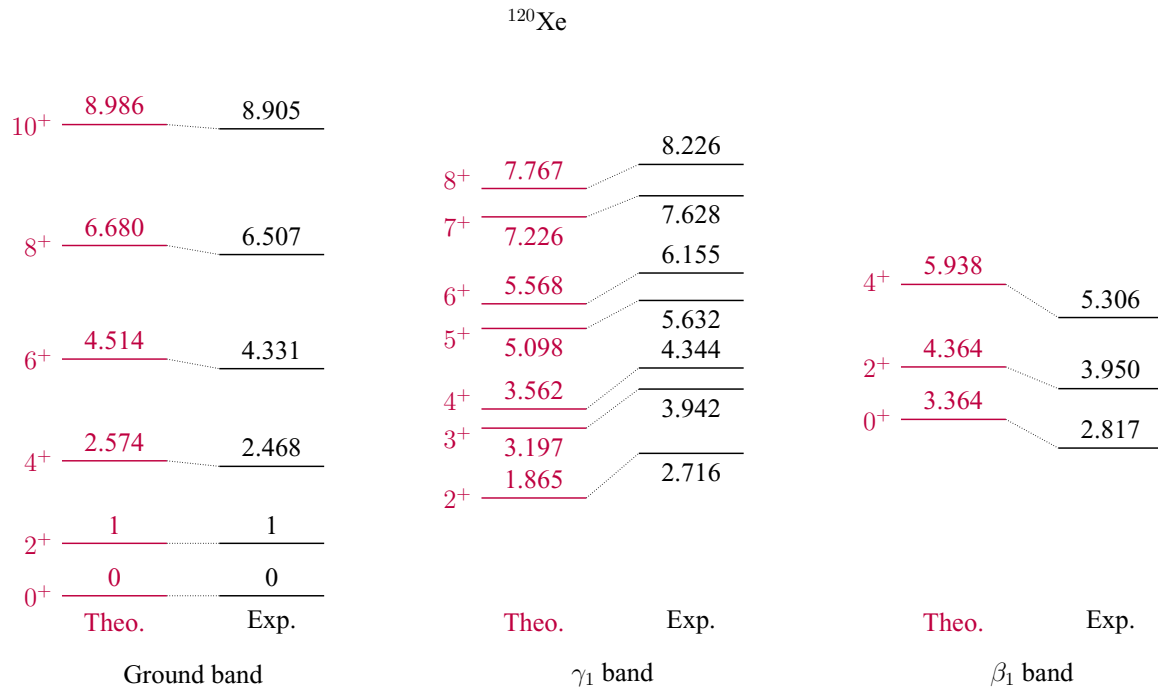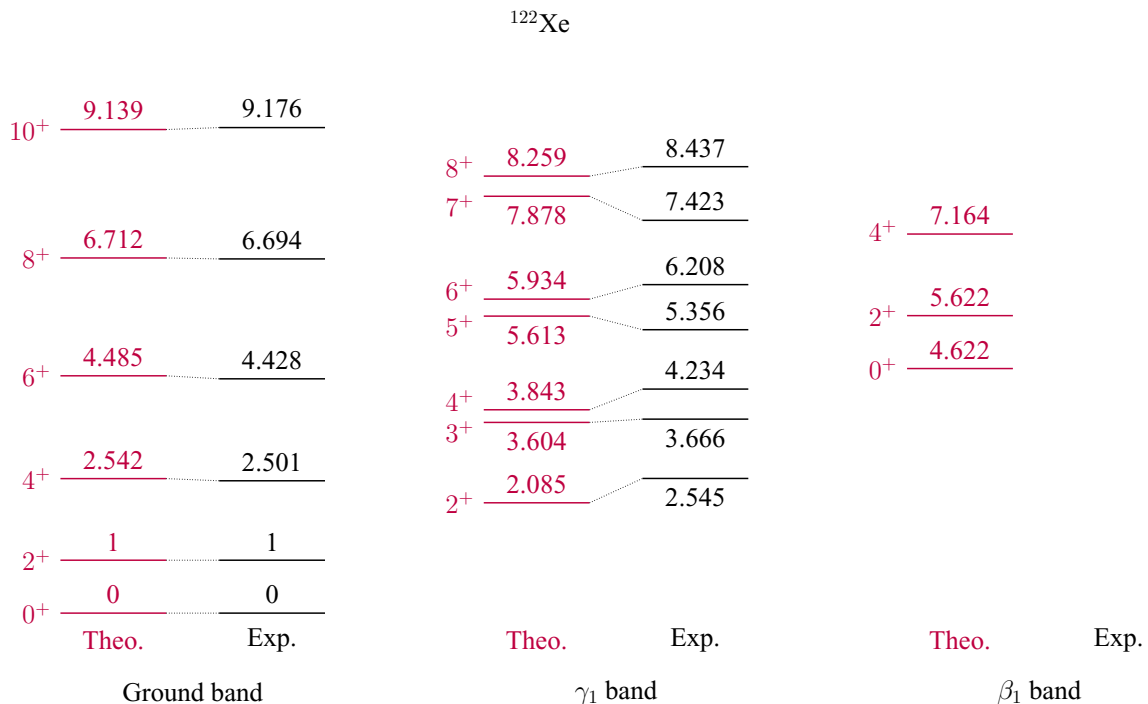
FIG. 4. Energy scheme of ^{120}Xe. In the fitting process, we used the levels which are connected to their corresponding experimental values. Experimental data for the energy levels were taken from Ref. [21]. The values have been normalized to the first excited levels of the ground band.

Eq. (12), has values of zero, and other quantum numbers such as the seniority and angular momentum can be determined by using the lower plot of Fig. 1. We know that each value of the seniority can correspond to some angular momentum. Thus we have connected these levels using a dotted line. The third box in the figure belongs to the first β band because in this band

FIG. 5. Energy scheme of ^{122}Xe. In the fitting process, we used the levels which are connected to their corresponding experimental values. Experimental data for the energy levels were taken from Ref. [21]. The values have been normalized to the first excited levels of the ground band.
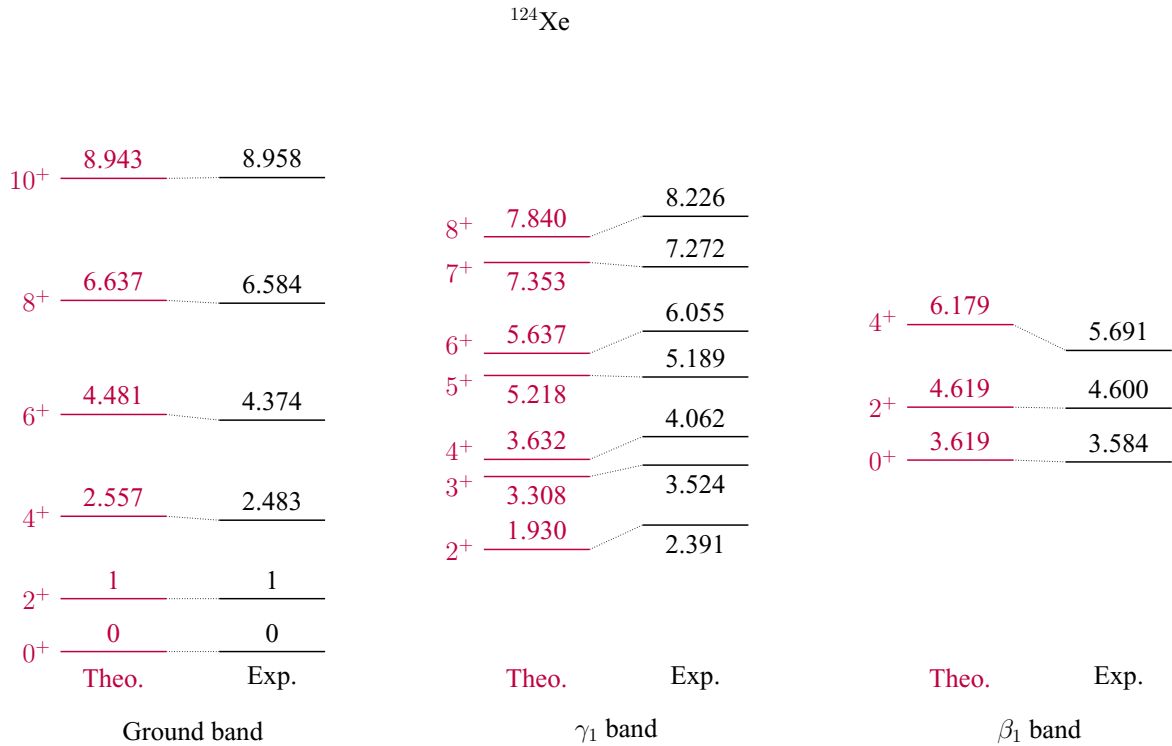
^{124}Xe

FIG. 6. Energy scheme of ^{124}Xe. In the fitting process, we used the levels which are connected to their corresponding experimental values. Experimental data for the energy levels were taken from Ref. [21]. The values have been normalized to the first excited levels of the ground band.

the quantum numbers for the β variable increase by one unit and the algorithm of its excited levels is the same as for the ground band. One can see that some other levels remain. It can be easily checked that other excited bands such as second or third bands of γ and β can be shown by considering higher

values of the seniority. We list the quantum numbers of each level in Table I.

Now, we are ready to present the numerical results according to the classifications of different bands. We used the least root mean square (rms) method to fit the theoretical predictions
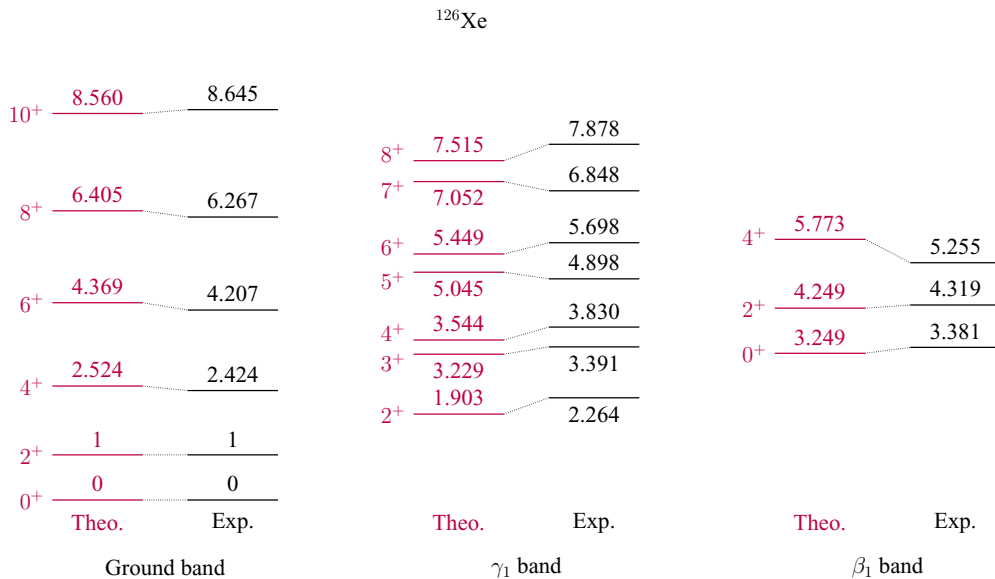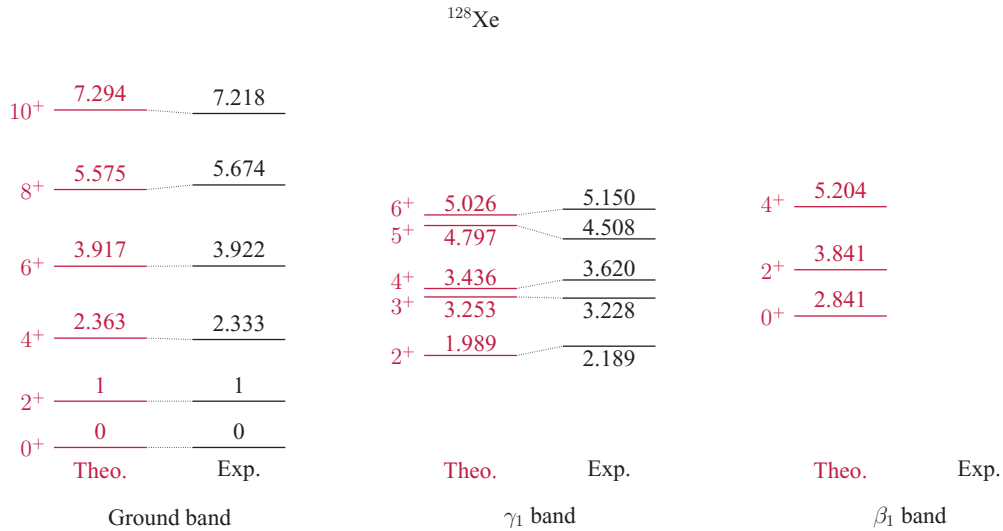
^{126}Xe

FIG. 7. Energy scheme of ^{126}Xe. In the fitting process, we used the levels which are connected to their corresponding experimental values. Experimental data for the energy levels were taken from Ref. [21]. The values have been normalized to the first excited levels of the ground band.

^{128}Xe

FIG. 8. Energy scheme of ^{128}Xe. In the fitting process, we used the levels which are connected to their corresponding experimental values. Experimental data for the energy levels were taken from Ref. [21]. The values have been normalized to the first excited levels of the ground band.

for the energy spectra of the ground, γ, and β bands on the experimental data. In this method, we should find the least deviation

$$\sigma = \sqrt{\frac{1}{N-1} \sum_{i=1}^{N} \left(\frac{E_i^{\text{expt}}}{E_{2^+}^{\text{expt}}} - \frac{E_i^{\text{theor}}}{E_{2^+}^{\text{theor}}} \right)^2}, \qquad (25)$$

where N stands for the number of states, and E_i^{expt} and E_i^{theor} represent experimental and theoretical energies of the ith level, respectively. During the derivation of the energy eigenvalue relation, in addition to the energy eigenvalue relation, we derived a constraint on the potential constants relating two of them together. It is important to note the constant "a" is not redundant. However, we cannot find the numerical values of the constants in one step. Actually, the real free parameters in our paper are κ, η, and b. These constants are determined in the numerical procedure of fitting. The constraint on the potential constant made a a function of b. It can be seen that since b is a scaling coefficient for Eq. (23), it can be canceled out without being determined. Therefore, in the first step, we
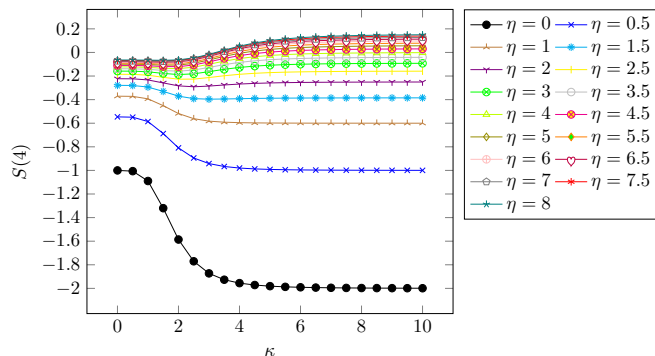
are able to determine only the numerical values of η and κ for the energy schemes using the rms method for each isotope. But we still calculate $B(E2)$ transitions rates. As is clear, the wave function depends on the free parameters a and b which are in the bi-confluent Heun function parameters. Equation (23) shows that if we determine b then a will be determined. Then we should use another fitting procedure for the $B(E2)$ transition rate to obtain the numerical value of b for each isotope. In other words, to determine the free parameters for each isotope, we need a two-step fitting process. The first step is finding η and κ using the energy scheme for each isotope. The second step is finding the least deviation for the $B(E2)$ transition rates for finding the numerical value of b for each isotope.

Before reproducing some experimental data, we want to check the asymptotic behavior of our considered model. The key signature is the ratio of $\frac{4_g}{2_g}$. In Fig. 2, we plotted the ratio
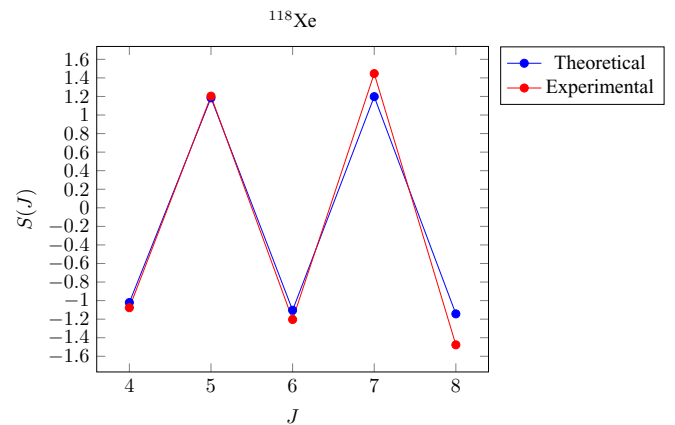

FIG. 9. $S(4)$ as a function of the free parameters κ and η.

FIG. 10. Comparison between the theoretical prediction and experimental staggering for ^{118}Xe.

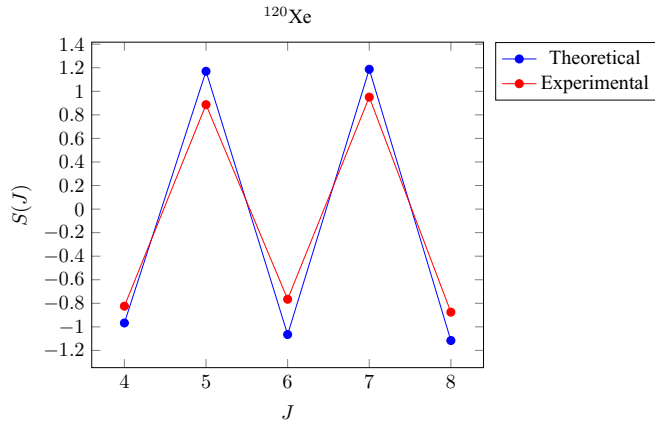FIG. 11. Comparison between the theoretical prediction and experimental staggering for ^{120}Xe.

FIG. 13. Comparison between the theoretical prediction and experimental staggering for ^{124}Xe.

of $\frac{4_g}{2_g}$ using Eq. (24) as a function of κ for different values of η. It is seen that the ratio of $\frac{4_g}{2_g}$ reaches a maximum value after certain values of κ and η. At first glance, we can find out that this model can recover the vibrator up to γ-soft nuclei. This figure shows that, considering large enough values of κ and η, we can approach the realm of the axially symmetric rotor where $\frac{4_g}{2_g} = 3.3$ but it will be seen that there is another quantity that does not allow the model. We selected some xenon isotopes (^{118,120,122,124,126,128}Xe). All experimental values were taken from Ref. [21]. In the fitting process, we found the best values for the free parameters that yielded the most minimal deviation. These values are listed in Table II for each isotope. We plotted the energy scheme of these isotopes in Figs. 3–8. In these figured, we separated the energy scheme of each isotope. We connected the corresponding levels between theoretical and experimental prediction by a dotted line. These levels have been contributed to the fitting process.

There is a useful quantity that is often known experimentally or is easy to measure in new nuclei to distinguish between axial symmetry and deviations from axial symmetry empirically. It is known as the energy staggering in the γ bands. It is a very
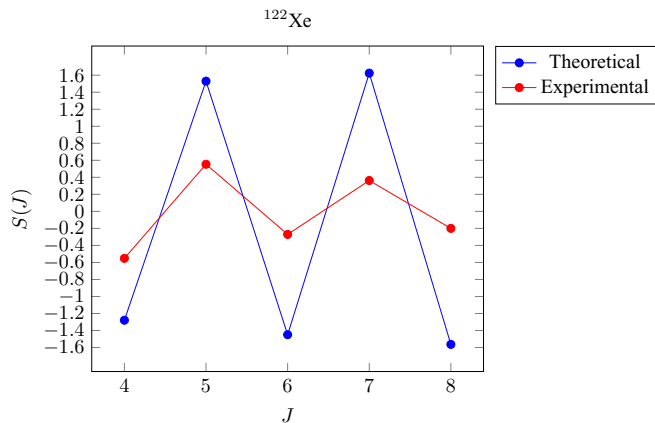
sensitive measure of the energy spacing. It is known that such an effect may appear due to mixing between the ground and γ-band levels with even angular momenta [22]. Staggering in γ bands is studied using the quantity [23,24]

$$S(J) = \frac{(E(J_\gamma^+) - E(J-1)_\gamma^+) - (E(J-1)_\gamma^+ - E(J-2)_\gamma^+)}{E(2_g^+)},$$

(26)

which measures the displacement of the $(J-1)_\gamma^+$ level relative to the average of its neighbors, J_γ^+ and $(J-2)_\gamma^+$, normalized to the energy of the first excited state of the ground band, 2_g^+. It is instructive if we study the asymptotic behavior of $S(4)$ using Eq. (23). It was shown in Fig. 2 that, for enough large values of κ and η, approaching the axially symmetric rotor realm can be possible but Fig. 9 make this point impossible. The $S(4)$ value for an axially symmetric rotor is 0.33 but at the upper limit of our considered model, at most, we can reach 0.2, which makes this point impossible. Looking more closely at Fig. 9, it is seen that for $\eta < 3$, the treatment of $S(4)$ tends to a minimum value, but for $\eta > 3$, this quantity tends to a maximum value.
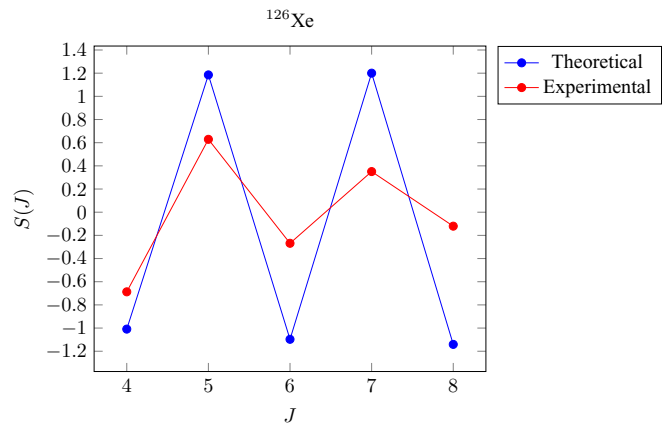

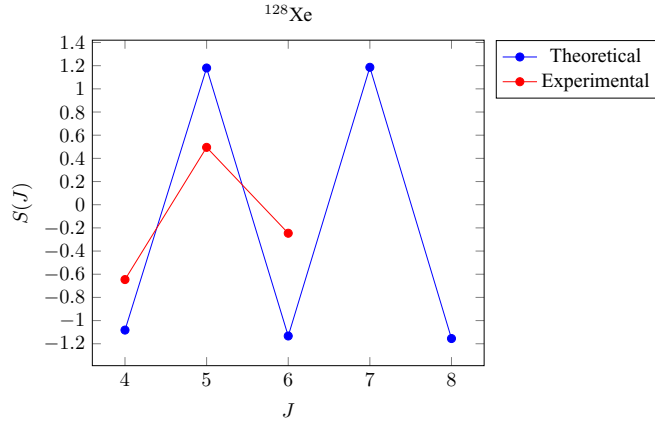FIG. 12. Comparison between the theoretical prediction and experimental staggering for ^{122}Xe.

FIG. 14. Comparison between the theoretical prediction and experimental staggering for ^{126}Xe.

FIG. 15. Comparison between the theoretical prediction and experimental staggering for ^{128}Xe.

The staggering has long been considered as theoretical staggering of different isotopes have been calculated and the results are shown in Figs. 10–15. For the cases of ^{118,120}Xe we can see a good theoretical prediction of staggering, but for the others, the agreement between theory and experiment become poor while we have found a good deviation for the energy level scheme for them. The reason is the contributing ground and β bands in addition to the contribution of the γ band to the fitting process. From Figs. 2 and 9, it would be good if one could find $\eta \approx 0.5$ for ^{122,124,126,128}Xe but in this case we could not find a good deviation.

Here we want to study the $E2$ electromagnetic transitions of the isotopes. The quadrupole transition operator can be expressed by [8,9]

$$T_\mu^{(E2)} = t\beta Q_\mu,$$
$$Q_\mu = D_{\mu 0}^2(\vartheta)\cos(\gamma) + \frac{1}{\sqrt{2}}\left(D_{\mu 2}^2(\vartheta) + D_{\mu -2}^2(\vartheta)\right)\sin(\gamma),$$
$$(27)$$

with the scaling factor t. Transition strengths are related to the reduced matrix elements by [25]

$$B(E2; n\tau L \rightarrow n'\tau'L')$$
$$= \frac{1}{\sqrt{2L+1}}|\langle n'\tau'L'|T^{(E2)}|n\tau L\rangle|^2,$$
$$= [t(\tau',L';1,2||\tau,L)A(\tau,\tau')I(n\tau L; n'\tau'L')]^2, \quad (28)$$

TABLE III. List of the numerical values for the free parameter b, evaluated by the fitting of theoretical predictions of $E2$ electromagnetic transition rates on the experimental values.

Isotope	b	$\sigma_{B(E2)}$
^{118}Xe	−300	0.912
^{120}Xe	−300	0.402
^{122}Xe	−300	0.460
^{124}Xe	−300	0.578
^{128}Xe	−98	0.511

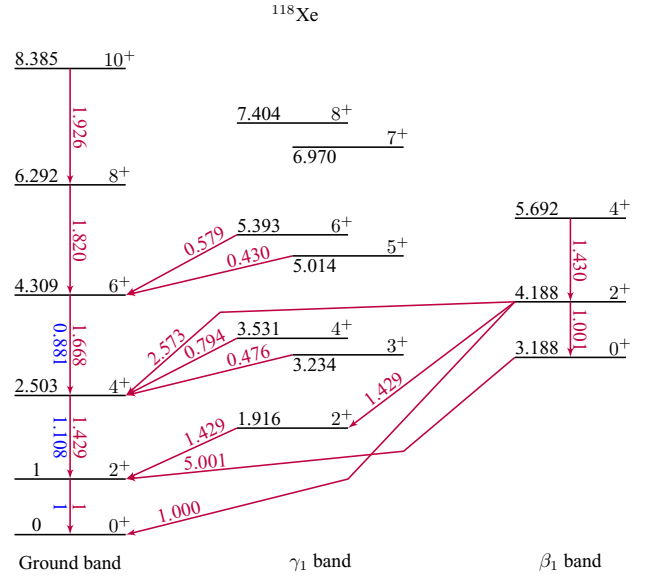
FIG. 16. $E2$ electromagnetic transition rate scheme of ^{118}Xe, shown by purple arrows which are normalized to $B(E2; 4_g \rightarrow 2_g)$.

$$A(\tau,\tau') = \sqrt{\frac{\tau}{2\tau+3}}\delta_{\tau,\tau'+1} + \sqrt{\frac{\tau+3}{2\tau+3}}\delta_{\tau,\tau'-1}, \quad (29)$$

$$I(n\tau L; n'\tau'L') = \int_0^\infty f_{n\tau L}(\beta)\beta f_{n'\tau'L'}(\beta)\beta^4 d\beta, \quad (30)$$

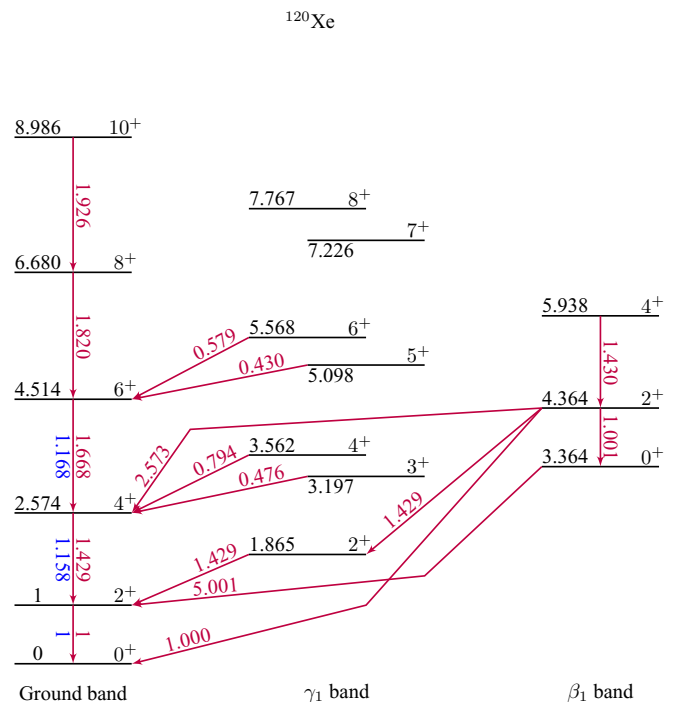where $(\tau',L';1,2||\tau,L)$ stands for the SO(5) Clebsch-Gordan coefficient dictating the angular momentum selection rules.

FIG. 17. $E2$ electromagnetic transition rate scheme of ^{120}Xe, shown by purple arrows which are normalized to $B(E2; 4_g \rightarrow 2_g)$.
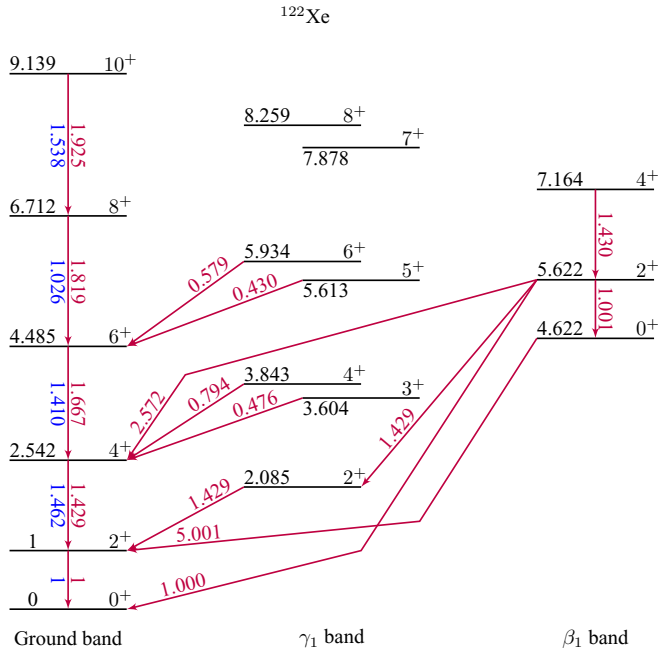
FIG. 18. $E2$ electromagnetic transition rate scheme of ^{122}Xe, shown by purple arrows which are normalized to $B(E2; 4_g \rightarrow 2_g)$.

Using Eq. (28), and Table II, we can calculate the $E2$ electromagnetic transition rates of each isotope. As we mentioned before, to calculate the $E2$ electromagnetic transition rates of each isotope, we need to evaluate the numerical value of b because it exists in a one-parameter bi-confluent Heun function [see Eqs. (18) and (19)]. We should use another fitting process to evaluate the numerical value of b resulting in finding the
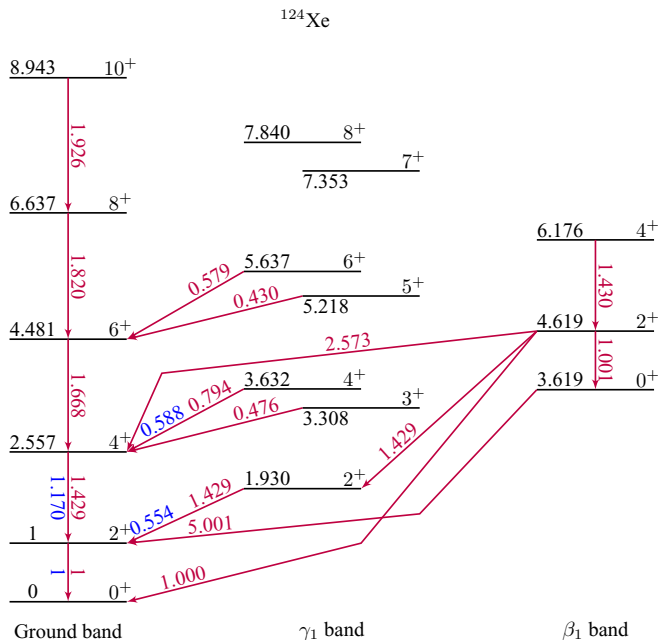

FIG. 19. $E2$ electromagnetic transition rate scheme of ^{124}Xe, shown by purple arrows which are normalized to $B(E2; 4_g \rightarrow 2_g)$.
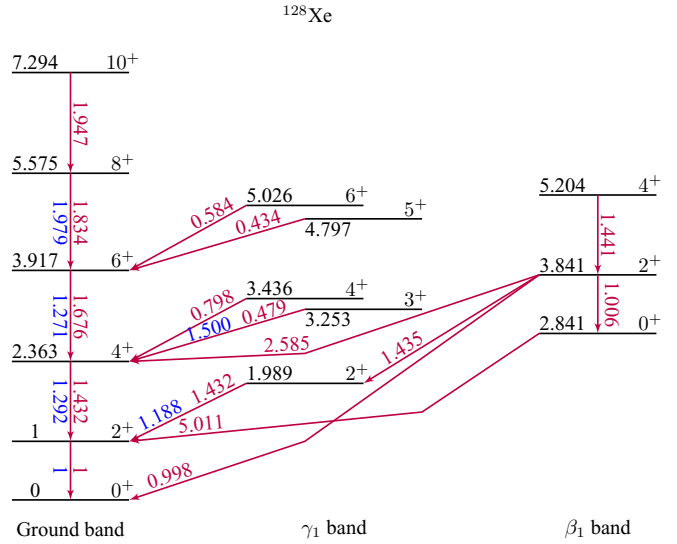

FIG. 20. $E2$ electromagnetic transition rate scheme of ^{128}Xe, shown by purple arrows which are normalized to $B(E2; 4_g \rightarrow 2_g)$.

numerical value of a. Using some experimental values for the $E2$ electromagnetic transition rates of considered isotopes, we find the numerical value of b for each isotope. The results are listed in Table III. Since there were not enough experimental data of $E2$ electromagnetic transitions for ^{126}Xe, we could not find the proper numerical value of b for these isotopes. Figures 16, 17, 18, 19, and 20 show the results of theoretical predictions for $E2$ electromagnetic transitions. The values mentioned in Fig. 20 have been normalized to $B(E2; 4_g \rightarrow 2_g)$. An important result of this figure is that in the absence of η, $B(E2; 4_g \rightarrow 2_g)$ and $B(E2; 2_\gamma \rightarrow 2_g)$ have the same value, but when we consider a nonzero value for η, it makes a difference between these $E2$ electromagnetic transition rates. As we mentioned before, the second step of fitting has taken place here. According to Table III, the best fit has been done for ^{120}Xe. Actually, this isotope can be considered the best candidate for the model considered in this paper.

As we claimed, the existence of η makes a difference in the values of the $E2$ electromagnetic transition rates. The reason for this difference is the angular dependence in the wave function. Although the Clebsch-Gordan coefficients follow the angular momentum selection rules, the existence of η in the wave function affects the overlap between the levels. The theoretical predictions for $E2$ electromagnetic transition rates are shown by purple arrows which are normalized to $B(E2; 4_g \rightarrow 2_g)$ in Fig. 20. These values are obtained by using Eqs. (21) and (28) and Tables II and III. The blue numbers are experimental values reported in Ref. [21].

IV. CONCLUSION

In this paper, we studied a general form of the γ-unstable Bohr Hamiltonian in the presence of a sextic potential. A general form means that in the considered system we included the effect of the Casimir operator of SO(3), which could eliminate the degeneracy of the degenerate levels. The wave function and energy eigenvalues were derived using

bi-confluent Heun functions. Then, to examine the results, we first discussed how we can characterize the ground, γ, and β bands; then we used some isotopes of xenon to reproduce their experimental data for energy and $E2$ electromagnetic transitions. The numerical results were evaluated after two fitting processes because two of the free parameters were determined in the fitting of energy levels and the last one was determined in the $E2$ electromagnetic transition. The results showed a good agreement with the experimental data.

[1] A. Bohr, Mat. Fys. Medd. K. Dan. Vidensk. Selsk. **26**, 14 (1952).

[2] A. Bohr and B. R. Mottelson, Mat. Fys. Medd. K. Dan. Vidensk. Selsk. **27**, 16 (1953).

[3] A. Bohr and B. R. Mottelson, *Nuclear Structure Vol. II: Nuclear Deformations* (Benjamin, New York, 1975).

[4] F. Iachello and A. Arima, *Interacting Boson Model* (Cambridge University Press, Cambridge, U.K., 1987).

[5] F. Iachello, Phys. Rev. Lett. **87**, 052502 (2001).

[6] R. F. Casten and N. V. Zamfir, Phys. Rev. Lett. **87**, 052503 (2001).

[7] F. Iachello, Phys. Rev. Lett. **91**, 132502 (2003).

[8] D. Bonatsos, D. Lenis, N. Minkov, D. Petrellis, P. P. Raychev, and P. A. Terziev, Phys. Rev. C **70**, 024305 (2004).

[9] D. Bonatsos, D. Lenis, N. Minkov, D. Petrellis, P. P. Raychev, and P. A. Terziev, Phys. Lett. B **584**, 40 (2004).

[10] L. Fortunato and A. Vitturi, J. Phys. G: Nucl. Part. Phys. **30**, 627 (2004).

[11] M. A. Caprio, Phys. Rev. C **65**, 031304 (2002).

[12] L. Fortunato and A. Vitturi, J. Phys. G **29**, 1341 (2003).

[13] G. Lèvai and J. M. Arias, Phys. Rev. C **69**, 014304 (2004).

[14] D. Bonatsos, D. Lenis, and D. Petrellis, Rom. Rep. Phys. **59**, 273 (2007).

[15] R. F. Casten and N. V. Zamfir, Phys. Rev. Lett. **85**, 3584 (2000).

[16] F. Iachello, Phys. Rev. Lett. **85**, 3580 (2000).

[17] H. Sobhani, A. N. Ikot, and H. Hassanabadi, Eur. Phys. J. Plus **132**, 240 (2017).

[18] M. A. Caprio and F. Iachello, Nucl. Phys. A **781**, 26 (2007).

[19] A. Ronveaux, *Heun's Differential Equations* (Oxford University Press, Oxford, U.K., 1986).

[20] H. Sobhani, H. Hassanabadiand, and W. S. Chung, Nucl. Phys. A **973**, 33 (2018).

[21] http://www.nndc.bnl.gov/ensdf/DatasetFetchServlet

[22] N. Minkov, S. B. Drenska, P. P. Raychev, R. P. Roussev, and D. Bonatsos, Phys. Rev. C **61**, 064301 (2000).

[23] N. V. Zamfir and R. F. Casten, Phys. Lett. B **260**, 265 (1991).

[24] E. A. McCutchan, Dennis Bonatsos, N. V. Zamfir, and R. F. Casten, Phys. Rev. C **76**, 024306 (2007).

[25] R. Budaca, Eur. Phys. J. A **52**, 314 (2016).